Special Article – New Tools and Techniques

High Efficiency Total Absorption Spectrometer HECTOR for capture reaction measurements

C.S. Reingold[1], O. Olivas-Gomez[1], A. Simon[1,a], J. Arroyo[1], M. Chamberlain[1], J. Wurzer[1], A. Spyrou[2,3], F. Naqvi[1], A.C. Dombos[2,1], A. Palmisano[2,3], T. Anderson[1], A.M. Clark[1], B. Frentz[1], M.R. Hall[1], S.L. Henderson[1], S. Moylan[1], D. Robertson[1], M. Skulski[1], E. Stech[1], S.Y. Strauss[1], W.P. Tan[1], and B. Vande Kolk[1]

[1] Department of Physics and Joint Institute for Nuclear Astrophysics, University of Notre Dame, Notre Dame, IN 46556, USA
[2] National Superconducting Cyclotron Laboratory, Michigan State University, East Lansing, MI 48824, USA
[3] Department of Physics and Astronomy, Michigan State University, East Lansing, MI 48824, USA

Abstract. Proper understanding of the stellar nucleosynthesis processes requires information on a variety of capture reaction cross sections. Since these cross sections are typically very low, they require efficient measurement techniques. The High Efficiency Total Absorption Spectrometer (HECTOR) was designed to measure capture cross sections relevant for astrophysical processes. HECTOR is a γ-summing detector comprised of 16 separate NaI(Tl) segments. The detector design is presented, as well as a detailed study of the detector's summing efficiency and analysis procedure. The results of the commissioning of HECTOR are presented. The resonance strengths of the well-known resonances in the ^{27}Al$(p, \gamma)^{28}$Si reaction measured with HECTOR are compared with the literature values.

1 Introduction

Radiative capture cross sections for heavy nuclei are key to understanding stellar nucleosynthesis. However, measurements of these cross sections can pose an experimental challenge as cross sections in the astrophysically relevant energy range are typically very small. In addition, structure information for nuclei relevant to astrophysical processes is, in many cases, incomplete. This missing structure information severely limits instances where γ-ray detection can be applied to studying capture reaction cross sections.

Typical measurements of proton- or α-capture reactions for stellar nucleosynthesis are performed using either the in-beam technique or the activation technique. The in-beam technique [1–3] employs high-resolution γ-ray detectors to measure γ rays following the de-excitation of an excited state populated during the reaction. In order to extract a cross section, the branching ratios of all the γ rays that populate the ground state need to be well known, and the angular distribution of the emitted γ rays must be determined. This technique proves to be particularly challenging for heavy nuclei, where the level schemes are not well known. As a result, transitions with low branching ratios or those that result in low-intensity γ rays feeding

into the ground state are overlooked. Thus, this technique frequently results in an underestimation of the cross section.

The activation technique [4–6] also has its limitations. For example, this technique is only applicable to the cases where the reaction product is unstable, with an appropriate half-life, typically minutes to days. The decay radiation of the reaction product also needs to be known to correctly account for the branching ratios.

The γ-summing technique [7,8] overcomes many of these difficulties. Since the detectors employed for these types of experiments cover nearly the full 4π solid angle, a correction for the angular distribution is not necessary. A well defined level scheme for the compound nucleus is also unnecessary, since the method depends on the averaged quantities of the γ-emission properties.

In this paper, HECTOR, a new γ-summing detector with full segmentation, will be discussed. In sect. 2, the principles of the γ-summing technique are explained. In sect. 3, the detector design and the data acquisition system are discussed. In sects. 4–7, the details of the summing technique, the data analysis procedure, and the procedure for calculating the detector summing efficiency are presented. In sect. 8, the first measurements performed using HECTOR for well-known resonances in the ^{27}Al$(p, \gamma)^{28}$Si reaction are compared with the literature values.
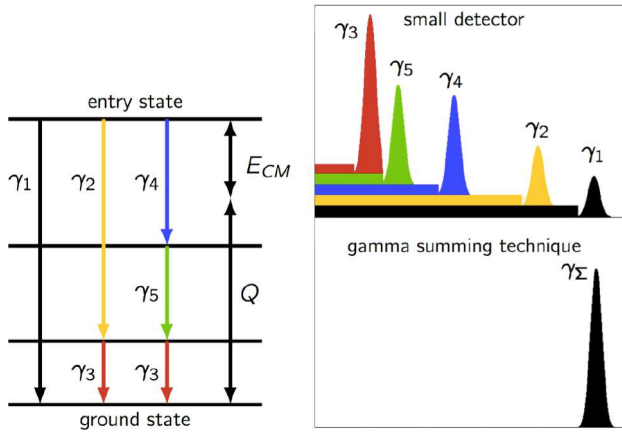
a e-mail: anna.simon@nd.edu

Fig. 1. A cartoon demonstrating the principles of the summing technique. For an arbitrary level scheme (left), there are many possible decay paths feeding the ground state. Instead of observing each of these γ rays individually (top right), the γ-summing technique (bottom right) measures the energy of an entire cascade. This eliminates the need for precise structure and branching information to be known about the compound nucleus.

2 γ-summing technique

The principle of the γ-summing technique is shown in fig. 1. The entry state populated by the captured projectile de-excites via emission of γ rays. When a small, high resolution detector is employed, the individual γ rays are detected, and the Compton background may hinder some of the lower intensity transitions. However, if a detector with 4π solid angle is used, the γ rays from each decay cascade are simultaneously detected and summed within the electronics to form a single peak at an energy E_Σ given by

$$E_\Sigma = E_{CM} + Q, \tag{1}$$

where E_{CM} is the center-of-mass energy of the projectile-target system, and Q is the reaction Q-value.

The angular coverage of the detector ensures a high summing efficiency (typically 10–30% for medium- and high-Z targets). This not only facilitates the rate at which data can be taken, but also allows for extending the measurement to much lower cross sections than are typically accessible via other techniques.

The γ-summing technique is a well established method for measurement of capture cross sections for heavy nuclei. The technique has been employed by Yamamoto *et al.* [9] using a 4π BGO total absorption detector for (n, γ). Another 4π BGO spectrometer for the summing technique has been developed for astrophysically relevant radiative capture reactions at the underground laboratory LUNA by C. Casella *et al.* [10]. The Karlsruhe 4π BaF detector [11] has also successfully employed the γ-summing technique to measure (n, γ) reactions.

Tsagari *et al.* [7] were able to use a large volume single NaI(Tl) crystal to perform total absorption spectroscopy for charged particle capture reactions. The next iteration of NaI(Tl) summing detector, SuN [12], introduced a segmentation of the crystal. Segmentation allows for Doppler
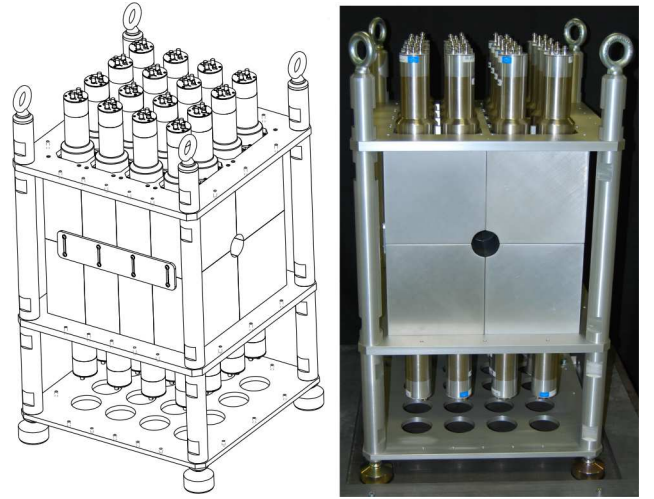

Fig. 2. The design for HECTOR (left), and a photograph of the actual detector (right).

correction of reaction γ rays, therefore allowing for the application of the summing technique to cross sections measured in inverse kinematics [13].

3 HECTOR

The High EffiCiency TOtal absorption spectrometeR (HECTOR) was designed at the University of Notre Dame, and manufactured by Saint-Gobain Crystals [14]. The array consists of 16 NaI(Tl) crystals, each with dimensions of $4'' \times 8'' \times 8''$. Scintillation light from each crystal is read out by two photomultiplier tubes. Each segment of HECTOR is housed by a 1 mm aluminum casing. The crystals are assembled to form a $16''$ cube. A 60 mm bore hole through the array allows for placing the target in the center of the array without compromising the solid angle covered by the detector. A schematic of the detector is shown in fig. 2.

The segmented design of HECTOR allows for simultaneous measurement of the total absorption spectrum and the individual γ rays contributing to the cascade. Therefore, some structure information from the de-excitation of the compound nucleus can be deduced from spectra measured with HECTOR. The modular design also allows for the possibility of coupling HECTOR to another array, or rearranging the segments to adapt to different target chambers.

During experiment, data from HECTOR is read out through the NSCL Digital Data Acquisition System (DDAS) [15]. The HECTOR acquisition system is similar to the one used with the SuN detector [12] at the NSCL. It is comprised of three XIA Pixie 16 [16] modules which are 16-channels 14-bit 100 MSPS digitizers. Two modules read the signal directly from the photomultipliers while the third one is used for monitoring purposes. For the in-beam commissioning of the array (sect. 8), the third module was configured to read an external trigger signal and beam current.
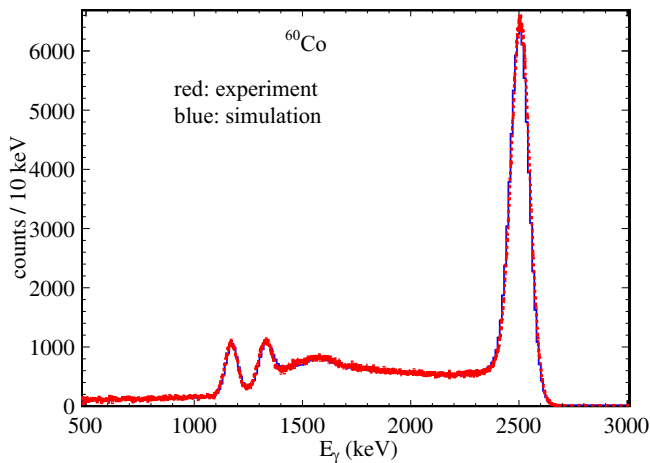
Fig. 3. Sum spectrum obtained for a ^{60}Co source located in the center of the HECTOR array, compared to a Geant4 simulation.

Fig. 4. Example of the analysis procedure of the sum peak from a ^{60}Co source. A Gaussian plus a linear function (solid red line) is fitted to the sum peak (green), the linear component (dashed red line) is subtracted from the sum peak within $(E_\Sigma - 3\sigma, E_\Sigma + 3\sigma)$. The result is shown in black. The same region is then integrated to obtain the total number of events in the sum-peak range.

4 Geant4 simulation

The external trigger signal is an analog sum of one PMT signal from each of the segments. While the discriminator thresholds on each individual PMT are kept just above the noise level (about 20 keV), the external trigger signal is used for triggering the DAQ only for events with total energy deposited in the detector above an adjustable 1–2 MeV threshold. As such, the trigger discriminates low-energy background counts without limiting the dynamic range of individual segments.

The beam current is read off the beam pipe and target holder within the detector. The assembly is electrically insulated from the detector and the beam line in front of the array, and is utilized as a Faraday cup. The charge collected from the beam pipe is recorded by a current digitizer that outputs NIM pulses, which are then recorded in a Pixie channel. Thus, the beam current is constantly monitored during the experiment.

4 Geant4 simulation

The summing technique allows for measurements of proton- and α-capture reaction cross sections for nuclei with unknown level schemes. The efficiency of the summing detector, however, depends on both the energy of the sum peak and the multiplicity of the γ-ray cascade. Therefore, the summing efficiency (ε_Σ) of the detector has to be determined as a function of these two parameters. For this purpose, a Geant4 [17] simulation of the HECTOR array has been developed. The geometry of the detector, including the dead layers, as specified in the technical documentation provided by the vendor was included in the simulation.

The quality of the simulation was tested with a ^{60}Co source. A comparison of the sum spectrum obtained experimentally for the source placed in the center of the array with the one generated by Geant4 is shown in fig. 3. A very good agreement between the two spectra can be observed.
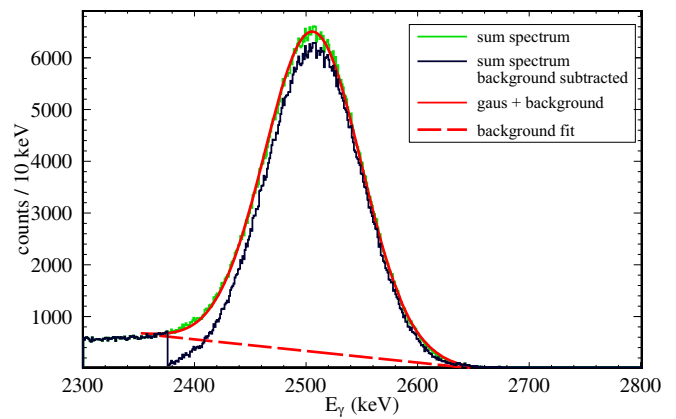
5 Data analysis procedure

Establishing a reliable, robust, and standardized analysis method for HECTOR is necessary for future cross-section measurements with the array. An important step of the data analysis is a proper subtraction of the background under the sum peak. The background under the sum peak includes room and cosmic-ray background, as well as events corresponding to incomplete summation of the γ rays of interest. In order to assess this background and eliminate it from the sum-peak integral, a standard procedure similar to those employed for other summing detectors [2,8] has been developed for HECTOR.

A two-step procedure is required to obtain robust and self-consistent background determination, as shown in fig. 4. The first step is a fit of a Gaussian function to the sum peak, excluding the background on the low-energy side of the peak, in order to determine the width (σ) of the sum peak and its position, $i.e.$, the sum-peak energy E_Σ. Once the width is determined, a region $(E_\Sigma - 3\sigma, E_\Sigma + 3\sigma)$ is fitted with a sum of a Gaussian function and linear background. The linear background is then subtracted from the spectrum and the region within $\pm 3\sigma$ from the peak centroid is integrated to obtain the total number of events in the sum peak. The uncertainties in the fit parameters are then propagated to obtain the uncertainty in the number of counts in the sum peak.

While the shape of the background under the sum-peak is more complex than a simple linear function, most likely has a form of a step function, the linear fit is more robust. In principle it rely only on two data points, at $E_\Sigma - 3\sigma$ and $E_\Sigma + 3\sigma$. Since the same procedure is applied to the experimental data and to Geant4 simulations for efficiency determination, the effects of systematic error introduced by this background subtraction are minimized.

The next step of the analysis is to determine the average multiplicity of the γ-ray cascade. This information
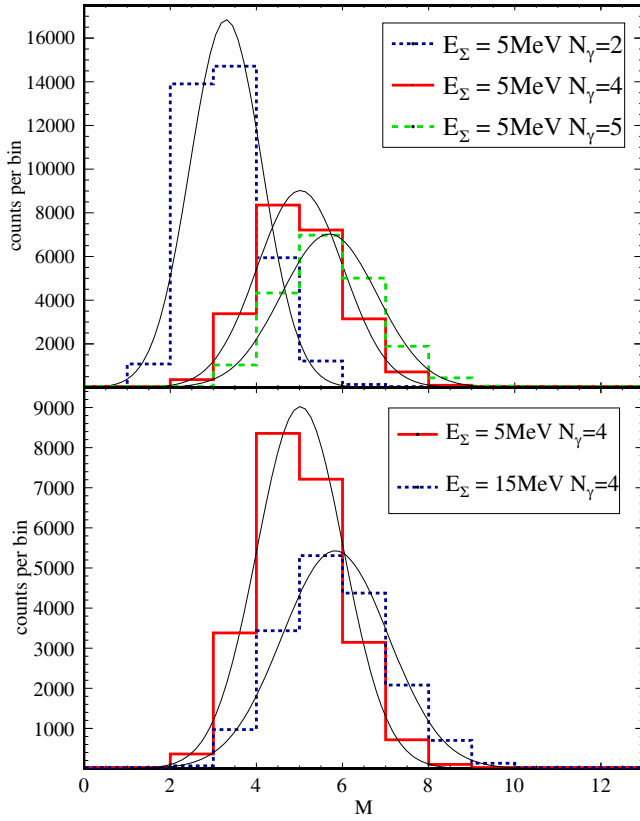
Fig. 5. Example hit patterns obtained from Geant4 simulations. Each pattern is generated by measuring the number of detectors fired for events within the sum-peak. Top panel: sum-peak energy of 5 MeV distributed evenly between γ rays of multiplicity 2, 4 and 5. Bottom panel: multiplicity 4 for the case of 5 and 15 MeV total energies. Gaussian curves fitted to the histograms are used to determine the average segment multiplicity $\langle M \rangle$.
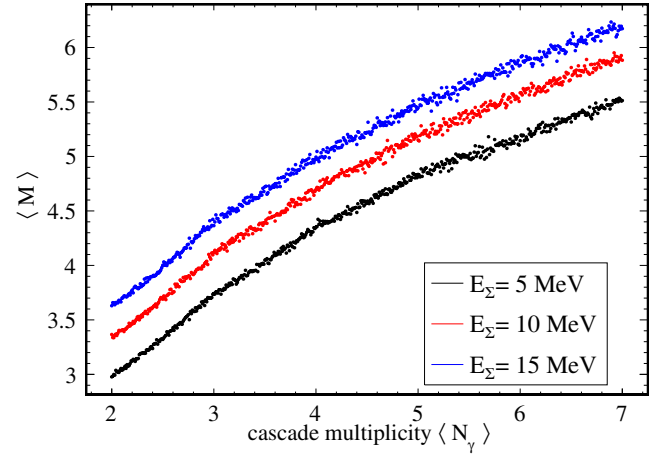

Fig. 6. Relation between the average number of γ rays in the cascade $\langle N_\gamma \rangle$, and the average segment multiplicity $\langle M \rangle$. Data obtained from Geant4 simulations (see sect. 6).

can be obtained two ways. The first one is to extract the average number of HECTOR segments that detected a γ ray for each event of a complete summation. The second one is the so-called "in/out" method [8] that compares the number of summation events in the whole detector array to those recorded in one half of the array.

A depiction of the first method is shown in figs. 5 and 6. The hit pattern is a histogram of the number of segments M that fired for events within the $\pm 3\sigma$ range of the sum peak. In fig. 5, sample hit patterns obtained from Geant4 simulations of γ-ray cascades are shown. A clear shift in the distribution can be seen for events with the same sum-peak energy but different γ-ray multiplicity, while a minimal shift in the distribution is observed for the same γ-ray multiplicity but different sum-peak energy. This is to be expected, as the number of interactions per γ ray does not change significantly within the energy region of interest. Thus, for cascades with a larger number of γ rays, the probability that the interaction involves a larger number of crystals increases. A plot of the hit pattern centroid $\langle M \rangle$ *versus* the average number of γ rays in a cascade $\langle N_\gamma \rangle$ as obtained from Geant4 simulations

for $E_\Sigma = 5$, 10, and 15 MeV is shown in fig. 6. The details of the aforementioned simulations are discussed in the following section.

The second method relies on the geometry of the γ-ray detection system. For example, suppose a γ-summing detector that covers a 4π solid angle was being used to measure a cascade with only one γ ray. The ratio of the sum peak intensity measured using the entire detector, relative to the intensity measured using only some fraction of the detector, would be proportional to the ratio of the solid angle coverage in each case. That is to say, the ratio of the sum-peak measured using the entire 4π detector ("in") relative to using only half the detector ("out") would be equal to two. For a cascade of N_γ γ rays, this ratio would instead be 2^{N_γ}. For a detector that does not cover a full 4π solid angle, like HECTOR, the base of the exponential is expected to be less than two. Additionally, for consistency with the method above, instead of N_γ, the number of segments M can be used. To determine the "in/out" ratio for HECTOR, the ratios of sum-peak intensities for simulated events of various combinations of E_Σ and $\langle M \rangle$ are shown in fig. 7. The "in/out" ratio for HECTOR is given as

$$R = 1.89(1)^{\langle M \rangle}, \tag{2}$$

where $\langle M \rangle$ is the hit pattern centroid. The results of this method are consistent with those of other summing detectors that use the "in/out" method to determine the average γ-ray multiplicity. In this work and in future ones, the first method will be used to determine $\langle M \rangle$ since in case of HECTOR it provides a better sensitivity to $\langle N_\gamma \rangle$ and as such allows for more precise determination of the summing efficiency.

6 Efficiency of the sum-peak

Determination of the summing efficiency (ε_Σ) of HECTOR is vital to the precision of cross sections measured
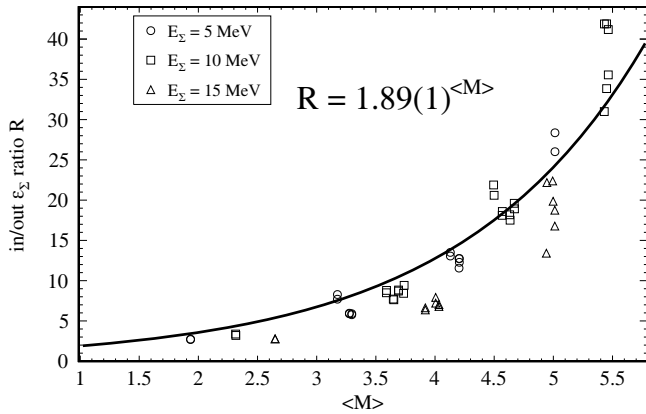
Fig. 7. Ratio of the efficiencies for the whole ("in") and half ("out") of the detector *vs.* the average segment multiplicity. Open symbols denote data from Geant4 simulation.

with the array. If the level scheme and branching ratios for a reaction of interest are known, then through Geant4, γ-cascades can be simulated and the resultant sum-peak fitted as discussed in the data analysis. The efficiency is then simply the ratio of the integral of the sum-peak to the number of cascade events simulated. However, as previously stated, the reactions of interest for nucleosynthesis processes involve nuclei for which the level scheme is unknown. In general, the summing efficiency depends both on the sum-peak energy and average number of γ rays in the cascade $\langle N_\gamma \rangle$. Although $\langle N_\gamma \rangle$ is likely not known for reactions of interest, the previous section has proven that there is a functional relation between $\langle N_\gamma \rangle$ and the average segment multiplicity $\langle M \rangle$ (fig. 6).

Therefore, to determine ε_Σ of the sum-peak, Geant4 simulations were performed for a fixed sum-peak energy, using cascades of varying numbers of γ rays. More specifically, each input file fed into the Geant4 simulations contained 100 different cascades, designed to mimic the complexity of a realistic cascade. For each cascade, the γ-ray energies were chosen from a uniform distribution under the constraint that the sum of the energies must equal the sum peak energy. In addition, no γ rays below 200 keV were selected, since the detection efficiency for γ-rays below this energy is very low. Additionally, within the resolution of the sum-peak, events for which the low-energy γ-ray was not detected will still be included in the sum-peak integral. Using combinations of these artificial cascades with different number of γ rays, we were able to sample different values for $\langle N_\gamma \rangle$. For example, a $\langle N_\gamma \rangle$ of 2.50 would contain 50 cascades of two γ-rays and 50 cascades of three γ rays. For each simulation, both the efficiency and $\langle M \rangle$ were extracted as outlined by the data analysis procedure (sect. 5). This procedure was repeated for a range deemed physically appropriate ($\langle N_\gamma \rangle = 2$ to $\langle N_\gamma \rangle = 7$). For each value of $\langle N_\gamma \rangle$ several realizations of the cascades were generated. This results in a slight spread of the $\langle M \rangle$ values and in the obtained efficiency values. This spread is an indication of the uncertainty in the summing efficiency. In fig. 8, three efficiency curve examples are plotted as a function of $\langle M \rangle$ for 5, 10, and 15 MeV sum-peak energies.
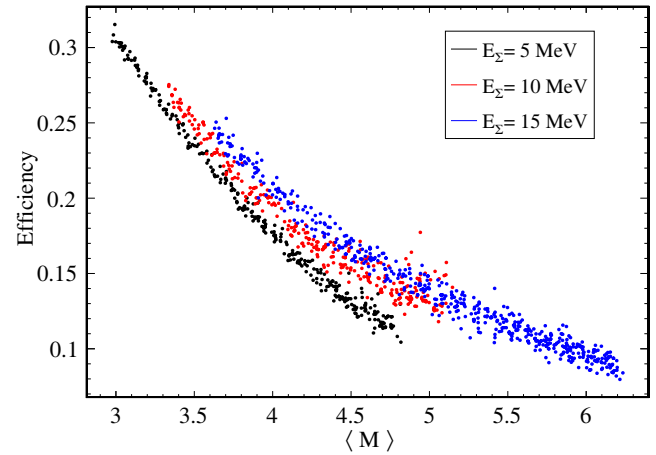

Fig. 8. Geant4 simulated summing efficiencies as a function of the average segment multiplicity $\langle M \rangle$. In general the summing efficiency depends on both the sum-peak energy and average cascade multiplicity $\langle N_\gamma \rangle$, but in the statistical limit, there is a one-to-one relation between $\langle N_\gamma \rangle$ and $\langle M \rangle$ which allows the efficiency to be estimated from $\langle M \rangle$.

As anticipated, the efficiencies decrease with increasing $\langle M \rangle$, which in general relates to an increasing $\langle N_\gamma \rangle$.

Finally, a second order polynomial was fit to the resultant efficiency curves, which is used to determine the efficiency for an experimentally measurable $\langle M \rangle$. The relative uncertainty in the efficiency is estimated by the relative scatter of the simulations, which is on the order of 10–20%.

7 Summing efficiency as a function of the source location along the borehole

In addition to the average segment multiplicity and the sum-peak energy, ε_Σ is also sensitive to the angular coverage of the detector. Therefore, ε_Σ is expected to depend on the location of the interaction point along the detector borehole, as this will change the amount of material the γ rays may interact with. For thin targets, which are placed in the center of the array, this location is well-known. However, if an extended gas cell is used as a target, this effect needs to be taken into account when calculating the cross section. Summing efficiency as a function of position along the borehole was investigated using a ^{60}Co source with known activity. The source was moved through the array using a wooden source holder, to both measure the position of the source, as well as to secure it within the array. The source was positioned in the center of the borehole, and moved along the borehole in 1 cm increments for the first 10 cm, and then in 2 cm increments until the source reached the edge of the array. For each source location, the summing efficiency for HECTOR was calculated. The results are displayed in fig. 9. Calculated ε_Σ values were then compared to two Geant4 simulations. When only HECTOR was accounted for in the simulation, the results overestimate the measurement. When the

Table 1. Average multiplicities ($\langle M \rangle$), summing efficiencies (ε_Σ) and resonance strengths (S_p) for ^{27}Al(p,γ)^{28}Si resonances analyzed in this work compared with the values from the literature.

E_p (keV)	E_Σ (MeV)	$\langle M \rangle$	ε_Σ	S_p (eV)				
				this work	Simon [12]	Endt [18]	NACRE [19]	Brenneisen [20]
2517.7	14.026	4.383	0.200(20)	16.9(10)	14.6(21)	16(3)	17.2(19)	15.9(32)
2675.5	14.141	4.564	0.187(20)	5.78(68)	4.7(10)	7.2(14)	7.32(84)	7.2(14)
2711.7	14.242	3.175	0.259(10)	18.1(11)	16.1(22)	14(3)	15.5(30)	13.9(28)
3098.0	14.455	4.426	0.177(20)	10.5(13)	–	6.7(13)	3.8(19)	6.7(13)
3338.4	14.681	4.492	0.172(20)	4.53(62)	3.6(7)	4.3(9)	4.2(8)	4.3(9)
3674.9	15.016	4.548	0.165(20)	35.1(45)	33.3(46)	35(7)	33.5(67)	34.7(69)
3791.7	15.265	4.401	0.192(20)	13.5(18)	11.9(16)	7.3(15)	7.1(17)	7.3(15)
3960.8	15.315	4.561	0.161(20)	5.92(81)	5.4(8)	3.3(7)	3.2(6)	3.3(6)
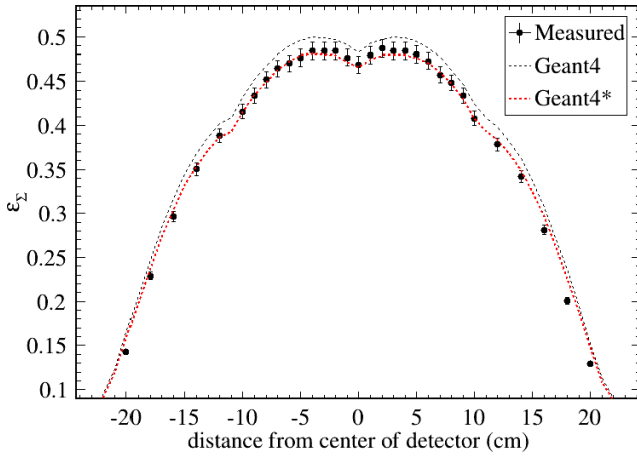
Fig. 9. Summing efficiency for a ^{60}Co source as a function of the position of the source along the detector borehole. The Geant4 curve (red, dashed line) includes the source holder in the simulation whereas the black-dashed line does not. Abrupt dips in efficiency correspond to the segmented gaps between crystals within the array.

source holder was added to the Geant4 simulations, there is good agreement between the measurement and simulations. This also shows that any additional material (*i.e.* target holder, collimator, etc.) can significantly affect the summing efficiency. Such materials need to be properly accounted for when determining the summing efficiency.

Additionally, it can be seen in fig. 9 that there are abrupt drops in the efficiency at 0 and ±10 cm. These positions correspond to the gaps between HECTOR segments. The gaps reduce the effective solid angle and consequently the summing efficiency.

8 Strength of the resonances in ^{27}Al(p,γ)^{28}Si reaction

The in-beam commissioning of HECTOR was performed by measuring well-known resonances in the ^{27}Al(p,γ)^{28}Si reaction. The commissioning experiment was conducted at the University of Notre Dame's Nuclear Science Laboratory.

Protons of energy range 2.5–4.2 MeV were generated using the FN Tandem Van de Graaff Accelerator. Each resonance was scanned in 1–2 keV energy steps in order to identify the energy centroid. The proton beam was incident on a 64.6(4) μg/cm^2, self-supporting aluminum target, which was manufactured at the Nuclear Science Laboratory as well. The target thickness was determined via the Rutherford backscattering technique using a 3.2 MeV ^{1}H, 4 MeV ^{4}He, and 8 MeV ^{12}C beams. Recoiled particles were detected using two silicon detectors at 135°, and 145° degrees. ^{241}Am and ^{148}Gd α-source emitters of 5,485 keV and 3,182 keV respectively were used to calibrate the detectors. The collected data was analyzed and fitted using SIMNRA [21].

The resonance strength S_p is defined as

$$S_p = \omega\gamma(2J_p + 1)(2J_t + 1), \qquad (3)$$

where J_p and J_t denote total projectile and target spin, respectively, and $\omega\gamma$ can be calculated from the integral of the excitation curve using the finite target thickness formula [8]

$$\omega\gamma = \frac{1}{\varepsilon_\Sigma}\frac{I_\gamma}{N_b}\frac{2}{\lambda_r^2}\frac{A}{N_A}\frac{M}{M+m}T(E_p) \qquad (4)$$

where I_γ is the intensity of the sum peak, λ_r is the de Broglie wavelength at the resonance energy, N_b is the number of beam particles incident on the target, ε_Σ is the summing efficiency, A is the atomic weight of the target, N_A is Avogadro's number, m and M are the beam and target masses, respectively, and $T(E_p)$ is the stopping power of the beam in the target.

Resonance strengths measured with HECTOR are listed in table 1. The de Broglie wavelength was calculated using the incident proton energy that was determined by an NMR probe measuring the magnetic field of the FN Tandem accelerator's 90° analyzing magnet. The intensity of the sum peak was obtained using the analysis procedure outlined in sect. 5 after the room background and non-resonant capture component were subtracted from the data. For each resonance, the summing efficiency was
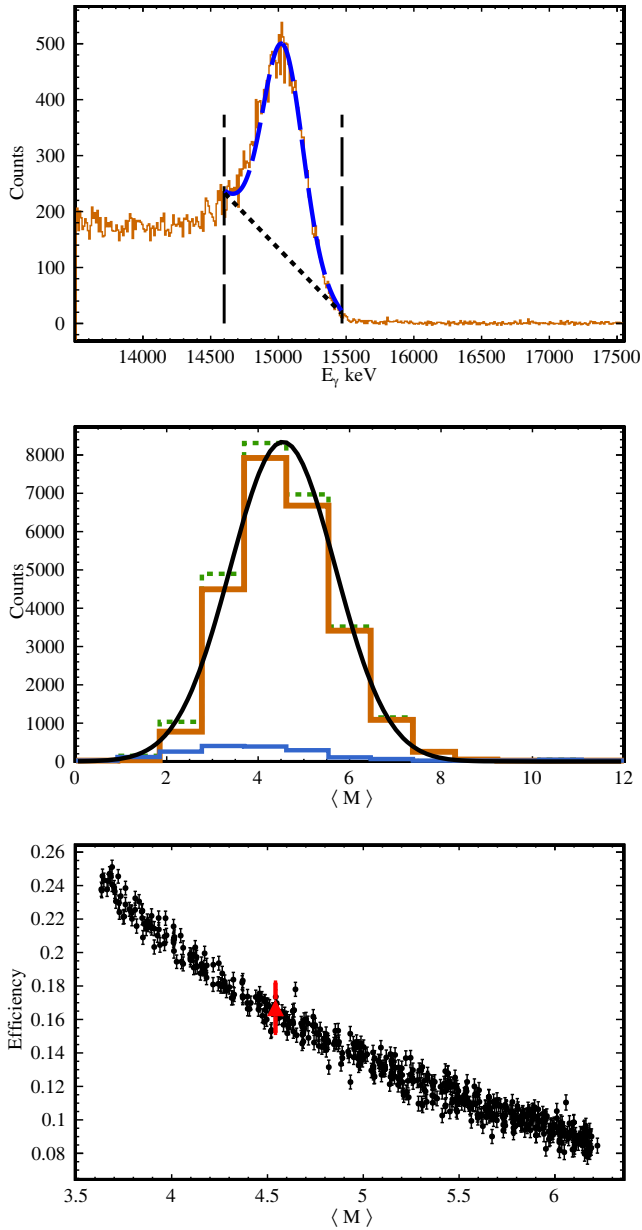
Fig. 11. Resonace strengths for the ^{27}Al$(p,\gamma)^{28}$Si reaction measured with HECTOR (solid data points), compared to SuN data [12] (open circles), Endt [18] (upside-down triangles), NACRE [19] (squares), and Brenneisen [20] (triangles). The results from HECTOR and SuN are in a very good agreement and reproduce well the data from other measurements.

tween our results and those listed in the literature. This agreement is especially strong with the results of Simon *et al.* [12], whose measurements were performed using the SuN detector which also applies the summing technique. The greatest discrepancy is in the 3,098 keV resonance, for which there is no summing technique literature value for comparison. However, for the resonances greater than 3 MeV, the resonance strengths measured in this work are consistently higher than those from evaluated sources such as NACRE [19] and Brenneisen *et al.* [20]. This discrepancy may be due to incomplete branching information used in their calculations.

The dominant term in the reported uncertainties arises from the error associated with estimating the summing efficiency which is on the order of 10% for the higher multiplicity resonances. Additional contributions to the resonance strength uncertainty include a 5% uncertainty in the target thickness, propagated through as an uncertainty in stopping power, as well as statistical errors associated with integrated quantities such as the beam current and sum peak intensity.

9 Summary

Measurements of radiative capture cross sections are important to the understanding of stellar nucleosynthesis. HECTOR, the newly commissioned γ-summing detector, will allow for such measurements to be conducted at the University of Notre Dame. HECTOR is comprised of 16 NaI(Tl) segments, with the γ-summing technique employed offline. The summing efficiency ε_Σ of HECTOR has been characterized as a function of average segment multiplicity $\langle M \rangle$ and sum-peak energy using Geant4 simulations. The calculated summing efficiency and standard analysis procedure outlined in this work have been tested by measuring ^{27}Al$(p,\gamma)^{28}$Si resonance strengths,

Fig. 10. Analysis of the 3,674 keV resonance in the ^{27}Al$(p,\gamma)^{28}$Si reaction measured with HECTOR, in the top figure, the sum peak is fitted, subtracted, and integrated within the 3σ region. In the middle figure a histogram of the segment multiplicities measured in the sum peak region is fitted. The smaller, blue historgram is off-resonance multiplicity, which is subtracted off. The bottom figure shows a simulated efficiency curve for a 15,240 keV sum peak. The average segment multiplicity is then compared to the efficiency curve to determine the sum-peak efficiency and uncertainty.

determined using a simulated efficiency curve as discussed in sect. 6. The procedure is demonstrated for the 3,674 keV resonance in fig. 10.

In total, eight resonance strengths were measured and are plotted in fig. 11 and listed in table 1 along with previous measurements found in the literature for comparison. In general, there is good agreement (within 1 σ) be-
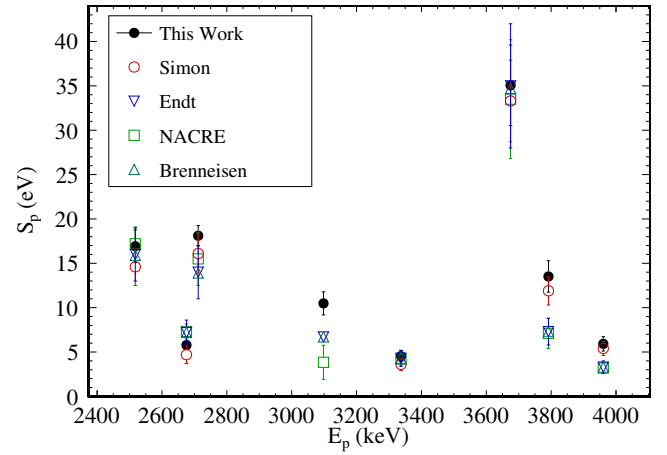
and comparing to literature values. The results are in good agreement with previous measurements, thus implying the aforementioned techniques are valid for measuring radiative capture cross sections. Future plans with the array include measuring (p, γ) and (α, γ) cross sections on stable, self-supporting targets, as well as developing a gaseous target system to study radiative capture on noble gas targets.

Data Availability Statement This manuscript has no associated data or the data will not be deposited. [Authors' comment: All data generated during this study are contained in this published article.]

Publisher's Note The EPJ Publishers remain neutral with regard to jurisdictional claims in published maps and institutional affiliations.

References

1. A. Sauerwein, J. Endres, L. Netterdon, A. Zilges, V. Foteinou, G. Provatas, T. Konstantinopoulos, M. Axiotis, S.F. Ashley, S. Harissopulos, T. Rauscher, Phys. Rev. C **86**, 035802 (2012).
2. S. Galanopoulos, P. Demetriou, M. Kokkoris, S. Harissopulos, R. Kunz, M. Fey, J.W. Hammer, G. Gyürky, Z. Fülop, E. Somorjai, S. Goriely, Phys. Rev. C **67**, 015801 (2003).
3. S. Harissopulos, A. Spyrou, A. Lagoyannis, M. Axiotis, P. Demetriou, J.W. Hammer, R. Kunz, H.W. Becker, Phys. Rev. C **87**, 025806 (2013).
4. M. Famiano, R.S. Kodikara, B.M. Giacherio, V.G. Subramanian, A. Kayani, Nucl. Phys. A **802**, 26 (2008).
5. N. Özkan, A. Murphy, R. Boyd, A. Cole, M. Famiano, R. Güray, M. Howard, L. Şahin, J. Zach, R. deHaan *et al.*, Nucl. Phys. A **710**, 469 (2002).
6. R.T. Güray, N. Özkan, C. Yalçın, T. Rauscher, G. Gyürky, J. Farkas, Z. Fülöp, Z. Halász, E. Somorjai, Phys. Rev. C **91**, 055809 (2015).
7. P. Tsagari, M. Kokkoris, E. Skreti, A.G. Karydas, S. Harissopulos, T. Paradellis, P. Demetriou, Phys. Rev. C **64**, 015802 (2004).
8. A. Spyrou, H.W. Becker, A. Lagoyannis, S. Harissopulos, C. Rolfs, Phys. Rev. C **76**, 015802 (2007).
9. S. Yamamoto, Y. Fujita, T. Shibata, S. Selvi, Nucl. Instrum. Methods A **249**, 484 (1986).
10. C. Casella, H. Costantini, A. Lemut, B. Limata, D. Bemmerer, R. Bonetti, C. Broggini, L. Campajola, P. Cocconi, P. Corvisiero *et al.*, Nucl. Instrum. Methods A **489**, 160 (2002).
11. K. Wisshak, K. Guber, F. Käppeler, J. Krisch, H. Müller, G. Rupp, F. Voss, Nucl. Instrum. Methods A **292**, 595 (1990).
12. A. Simon, S. Quinn, A. Spyrou, A. Battaglia, I. Beskin, A. Best, B. Bucher, M. Couder, P. DeYoung, X. Fang *et al.*, Nucl. Instrum. Methods Phys. Res. A **703**, 16 (2013).
13. S. Quinn, A. Spyrou, A. Simon, A. Battaglia, M. Bowers, B. Bucher, C. Casarella, M. Couder, P. DeYoung, A. Dombos *et al.*, Nucl. Instrum. Methods Phys. Res. A **757**, 62 (2014).
14. StGobain Crystals, `https://www.crystals.saint-gobain.com` (2019).
15. C. Prokop, S. Liddick, B. Abromeit, A. Chemey, N. Larsen, S. Suchyta, J. Tompkins, Nucl. Instrum. Methods A **741**, 163 (2014).
16. XIA LLC, `http://www.xia.com/DGF_Pixie-16.html` (2019).
17. J. Allison, K. Amako, J. Apostolakis, P. Arce, M. Asai, T. Aso, E. Bagli, A. Bagulya, S. Banerjee, G. Barrand *et al.*, Nucl. Instrum. Methods Phys. Res. A **835**, 186 (2016).
18. P.M. Endt, Nucl. Phys. A **633**, 1 (1998).
19. NACRE database, `http://pntpm.ulb.ac.be/Nacre/nacre.htm` (2019).
20. J. Brenneisen, D. Grathwohl, M. Lickert, R. Ott, R. Höpke, J. Schmälzlin, B. Wildenthal, Z. Phys. A **352**, 149 (1995).
21. M. Mayer, in *Report IPP 9/113, Max-Planck-Institut für Plasmaphysik* (Garching, Germany, 1997).